Characterization of Nonplanar Second Harmonic Lamb Waves with a Refined Nonlinear Parameter

Shengbo Shan, Li Cheng* and Fuzhen Wen

Department of mechanical engineering, The Hong Kong Polytechnic University, Kowloon, Hong Kong.

E-mail: li.cheng@polyu.edu.hk

Abstract

Structural health monitoring (SHM) methods based on the cumulative second harmonic Lamb waves show attractive advantages. An ideal nonlinear parameter should allow precise characterization of the cumulative effects of the distributed nonlinear sources such as the material nonlinearity of a plate (MNP), in the presence of other unavoidable localized nonlinear components. While highlighting the deficiencies of the traditional nonlinear parameter (*TNP*) in the nonplanar cases, a refined nonlinear parameter (*RNP*) is proposed. Through compensations for the wave attenuation associated with the wave divergence, the new parameter entails a better characterization and differentiation of the cumulative MNP and other non-cumulative localized nonlinear sources. Theoretical findings are ascertained by both finite element simulations and experiments, through tactically adjusting the dominance level of different nonlinear sources in the

system. Results confirm the appealing features of the proposed *RNP* for SHM applications.

Keywords: Second harmonic Lamb waves, cumulative effect, nonlinear parameter

1 Introduction

The nonlinear-Lamb-wave-based structural health monitoring (NL-SHM), a technology combining the advantages of both Lamb-wave-based inspections and nonlinear ultrasonics, has been gaining popularity in recent years. Taking Lamb waves as the information carrier, it is now possible to interrogate a large area of a thin-walled structure with a sparse sensor array for the real-time and online monitoring of its health status [1-3]. Meanwhile, owing to their high sensitivity to microstructural changes, nonlinear Lamb waves allow the early detection of the structural damage or even material degradations, facilitating the further maintenance decisions [4, 5].

Several nonlinear ultrasonic detection techniques have so far been developed, such as the nonlinear resonant ultrasound spectroscopy [6], nonlinear elastic wave spectroscopy [7, 8], and higher harmonic generations [9, 10], etc. Among all these techniques, the second harmonic generation in a plate before the initiation of cracks is of particular interest. The second harmonic Lamb waves can be generated by various nonlinear sources in a typical NL-SHM system, either distributed or localized in nature. The distributed one is typically the material nonlinearity of the plate (MNP), a damage-related nonlinear source which has been extensively investigated in previous studies [11-17]. Relevant to the material degradations, the MNP-induced second

harmonic Lamb waves exhibit the so-called cumulative effect when the synchronism conditions are satisfied: *i.e.* the match of the phase velocities between the first and the second harmonics and the non-zero power flux among them, resulting in a limited number of mode pairs that can be used for SHM [15]. Recently, the cumulative effect of the MNP-induced second harmonic S_0 mode Lamb waves has been shown to exist in the low-frequency range when the phase velocities approximately match [16]. Compared with the commonly used high-frequency mode pairs, the use of the S_0 mode Lamb waves in the low-frequency range is attractive for the SHM applications in terms of the flexibility it offers in choosing the excitation frequencies and the lower demand for the measuring equipment. Localized nonlinear sources, such as the instrumental nonlinearity, adhesive nonlinearity (AN) [18] and so on, are often considered as typical non-damage-related nonlinear sources. Generally speaking, the second harmonic Lamb waves induced by these localized nonlinear sources propagate independently in the plate, thus exhibiting the non-cumulative effect. Specifically, the influence of AN was shown to be inevitable and non-negligible in a typical piezoelectric wafer-actuated SHM system [18], which may exceed that of the instrumental nonlinearity. Therefore, AN is chosen as a typical example of the localized nonlinear sources, to be investigated in this paper.

Owing to its close relation to the MNP, the cumulative effect can naturally be used as an indicator of the distributed material degradations. Moreover, even though there are other localized nonlinear sources, their corresponding second harmonic Lamb waves are non-cumulative so that the MNP-induced cumulative feature will, in principle, not be affected by these localized nonlinear sources. This constitutes the most appealing advantage of the cumulative effect-based SHM methods in terms of their high tolerance to the non-damage-related nonlinear sources in the

system. To develop relevant SHM methods, it is usually required to examine the variation of the nonlinear parameter versus the propagating distance. The material status can then be monitored through tracking the slope of the nonlinear parameter versus propagating distance curve. The key for achieving this goal, therefore, strongly depends on a properly chosen nonlinear parameter. The ideal one should allow a clear characterization and differentiation of the distributed and localized nonlinear sources at the same time in terms of their cumulative effects. Otherwise, the presence of the localized nonlinear sources can seriously affect or even jeopardize the damage diagnosis in practice.

In the open literature, the so-called relative nonlinear parameter, commonly denoted by *β'*, is widely adopted [4, 16, 19-24]. For the ease of discussions, it is referred to as the traditional nonlinear parameter (*TNP*) in this paper, which is defined as

$$TNP = \beta' = \frac{A^{\mathrm{NL}}(2\omega)}{\left(A^{\mathrm{L}}(\omega)\right)^2} \tag{1}$$

where $A^{\mathrm{NL}}(2\omega)$ and $A^{\mathrm{L}}(\omega)$ are the amplitudes of the second harmonic and fundamental Lamb waves respectively. The amplitude of the wave components can be obtained from either displacement or any other sensor output [25]. Whatever is used, the relative nonlinear parameter allows tracking the changes of material status, in compliance with the SHM philosophy [21]. In the ideal scenario, the relative nonlinear parameter is independent of the excitation amplitudes, observable from its definition (in terms of the amplitude to the square of the amplitude ratio). Therefore, it is only related to the nonlinear system itself [4]. Due to these appealing characters, the *TNP* has been used for decades to characterize the second harmonic responses.

It is important to note that the concept of the *TNP* originates from the bulk wave case under the assumption that the amplitude of the fundamental waves remains unchanged during the wave

propagation process [4]. This may be irrelevant if the *TNP* is used to track the structural or material changes when the distance between the actuator and sensor is fixed. When it comes to the characterization of the cumulative effects of the second harmonic Lamb waves with the changing distances, however, this assumption, as well as its consequences in the SHM applications becomes questionable. In one-dimensional cases (1D cases), the plane wave theory can be roughly applied, as used in many theoretical and numerical investigations [12, 15, 16]. In these cases, the gradual increase in the amplitudes of the MNP-induced second harmonic Lamb waves result in an expected gradual increase in the *TNP*, since the propagating Lamb waves are non-diverging. In any practical SHM applications, however, Lamb waves are usually generated within a confined region by actuators of finite size such as piezoelectric wafers. Waves then propagate in a two-dimensional pattern (2D cases), becoming nonplanar and divergent so that their amplitudes decrease with the propagation distance. Therefore, the independence of the *TNP* on the amplitude of fundamental waves, established in 1D cases, may be compromised. As a result, the legitimacy of using the *TNP* to characterize the MNP needs to be re-examined. Moreover, due to the existence of some inevitable nonlinear sources in the system, particularly the AN, it is also crucial to examine whether the specific non-cumulative nonlinear source can be properly characterized by the *TNP*.

In this paper, the distributed MNP and the localized nonlinear sources like the AN in both 1D and 2D cases are characterized. Analyses first highlight the deficiencies of the *TNP* in 2D nonplanar applications. Then a refined nonlinear parameter is proposed based on the wave propagation characteristics for a better characterization of both the cumulative MNP-induced and the non-cumulative AN-induced nonlinear Lamb waves. Finite element (FE) simulations are

performed with the AN and the MNP being tactically separated in the models. Upon extracting the amplitudes of the time-domain signals using a peak tracking method, the *TNP* and the refined nonlinear parameter are compared in terms of their ability to characterize the second harmonic responses, which demonstrates the superiority of the proposed nonlinear parameter. Finally, a previously developed model [18] is used to guide the design of two experimental configurations, an optimized and an un-optimized. These purpose-driven experimental configurations are conceived to adjust the dominance level of the AN over the MNP to further assess the ability of the proposed parameter in dealing with these two types of nonlinear sources.

2 Theoretical analyses

Two important nonlinear sources, the distributed MNP and a representative localized AN, present in a typical NL-SHM system actuated by the piezoelectric wafers, are considered. Specifically, problems associated with the *TNP* for characterizing the second harmonic Lamb waves in the nonplanar 2D cases, are scrutinized. Based on the physical understandings revealed by the theoretical analyses, a refined nonlinear parameter is proposed, aiming at a better characterization and differentiation of the cumulative MNP-induced and the non-cumulative AN-induced second harmonic Lamb waves in the system.

2.1 Characterization of the AN-induced second harmonic Lamb waves with *TNP*. As shown in [18], the influence of the AN at the actuator-plate interaction is more significant than that at the sensing part in terms of the second harmonic responses. Therefore, analyses will mainly focus on

the adhesive layer over the actuation area. In an ideal 1D case, the AN-induced second harmonic Lamb waves propagate independently with the linear wave components. In the absence of the MNP and the wave attenuation, the amplitudes of both the linear and nonlinear Lamb waves remain unchanged during the propagation as sketched in Fig. 1(a). Using the *TNP*, the slope of the *TNP-x* curve should then be zero, with *x* being the propagation distance from the actuator. In addition, this zero-slope feature should be independent of the material nonlinear properties of the adhesive layers.

In practical 2D cases, the attenuation of Lamb waves can be mainly attributed to two factors: wave divergence and material damping. The present work mainly focuses on the S_0 mode Lamb wave propagation in an aluminum plate in the low-frequency range, within which the wave attenuation due to the material damping is much weaker than that due to the wave beam divergence. Therefore, the former, which is frequency-dependent in principle, is considered to be negligible. Of course, this will not be applicable to other more dissipative media such as composite plates. As far as the wave divergence is concerned, it has been shown that the amplitude of Lamb waves decreases as a function of the square root of the propagating distance, but independent of the frequencies [26]. Based on this and considering both the linear and the AN-induced Lamb waves, propagating from M to N through a direct path, one has

$$\frac{A_{\mathrm{N}}^{\mathrm{L}}(\omega)}{A_{\mathrm{M}}^{\mathrm{L}}(\omega)}=\frac{A_{\mathrm{N}}^{\mathrm{NL}}(2\omega)}{A_{\mathrm{M}}^{\mathrm{NL}}(2\omega)} \tag{2}$$

where $A(\omega)$ and $A(2\omega)$ are the amplitudes of Lamb waves at the fundamental and the double frequencies, respectively. Subscripts M and N denote the two positions under consideration and superscripts L and NL represent the linear and nonlinear wave components, respectively. Using *TNP*, the slope (*SL*) of the *TNP-x* curve writes

$$SL=\frac{\dfrac{A_{\mathrm{N}}^{\mathrm{NL}}(2\omega)}{\left(A_{\mathrm{N}}^{\mathrm{L}}(\omega)\right)^2}-\dfrac{A_{\mathrm{M}}^{\mathrm{NL}}(2\omega)}{\left(A_{\mathrm{M}}^{\mathrm{L}}(\omega)\right)^2}}{\Delta x}=\frac{A_{\mathrm{N}}^{\mathrm{NL}}(2\omega)}{A_{\mathrm{N}}^{\mathrm{L}}(\omega)}\cdot\frac{\dfrac{1}{A_{\mathrm{N}}^{\mathrm{L}}(\omega)}-\dfrac{1}{A_{\mathrm{M}}^{\mathrm{L}}(\omega)}}{\Delta x} \tag{3}$$

where Δx denotes the distance between the two points M and N. Eq. (3) shows a product of two terms in which the first one only involves the wave amplitudes, which is always positive. The same applies to the second term, since $A_{\mathrm{N}}^{\mathrm{L}}(\omega) < A_{\mathrm{M}}^{\mathrm{L}}(\omega)$ due to the 2D wave divergence. As a result, *SL* is always positive, giving an upward variation trend of the *TNP* with the propagation distance. This shows a false positive cumulative effect in the nonplanar 2D scenario, which should not exist in the absence of the MNP.

2.2 Characterization of MNP-induced second harmonic Lamb waves with *TNP*. Considering the damage-related MNP in the same low-frequency range, we focus on the cumulative MNP-induced S_0 mode Lamb waves. In 1D cases, the amplitudes of the linear wave components remain almost constant during the wave propagating while the nonlinear wave amplitudes gradually increase due to the distributed material nonlinearity, as illustrated in Fig. 1(b). Without loss of generality, the amplitude of the MNP-induced cumulative second harmonic Lamb waves at a position N can be expressed as

$$A_{\mathrm{N}}^{\mathrm{NL}}(2\omega)=A_{\mathrm{M}}^{\mathrm{NL}}(2\omega)+k_{\mathrm{material}}\left(A_{\mathrm{M}}^{\mathrm{L}}(\omega)\right)^2\Delta x \tag{4}$$

where k_{material} is a comprehensive parameter related to the material nonlinear properties at a specific excitation frequency. As $A_{\mathrm{N}}^{\mathrm{L}}(\omega)=A_{\mathrm{M}}^{\mathrm{L}}(\omega)$ in the present 1D case, the *SL* in the *TNP*-*x* figure can be expressed as

$$SL=\frac{\dfrac{A_{\mathrm{N}}^{\mathrm{NL}}(2\omega)}{\left(A_{\mathrm{N}}^{\mathrm{L}}(\omega)\right)^2}-\dfrac{A_{\mathrm{M}}^{\mathrm{NL}}(2\omega)}{\left(A_{\mathrm{M}}^{\mathrm{L}}(\omega)\right)^2}}{\Delta x}=\frac{\dfrac{A_{\mathrm{M}}^{\mathrm{NL}}(2\omega)+k_{\mathrm{material}}\left(A_{\mathrm{M}}^{\mathrm{L}}(\omega)\right)^2\Delta x}{\left(A_{\mathrm{M}}^{\mathrm{L}}(\omega)\right)^2}-\dfrac{A_{\mathrm{M}}^{\mathrm{NL}}(2\omega)}{\left(A_{\mathrm{M}}^{\mathrm{L}}(\omega)\right)^2}}{\Delta x}=k_{\mathrm{material}} \tag{5}$$

Eq. (5) shows a constant slope, which is only related to the material nonlinear elastic properties at a specific excitation frequency, in agreement with previous studies [15, 16].

In a nonplanar 2D case, when the linear and the MNP-induced Lamb waves propagate from M to N through a direct path, the amplitude of the second harmonic Lamb waves at N can be decomposed into two parts as

$$A_{\mathrm{N}}^{\mathrm{NL}}(2\omega)=A_{\mathrm{N1}}^{\mathrm{NL}}(2\omega)+\left[\int_{\mathrm{M}}^{\mathrm{N}} k_{\mathrm{material}}\left(A^{\mathrm{L}}(\omega)\right)^{2}\mathrm{d}x\right]f(x) \tag{6}$$

where the first part $A_{\mathrm{N1}}^{\mathrm{NL}}(2\omega)$ denotes the nonlinear wave amplitude without the cumulative effect. Analog to Eq. (2), one approximately has $\frac{A_{\mathrm{N}}^{\mathrm{L}}(\omega)}{A_{\mathrm{M}}^{\mathrm{L}}(\omega)}=\frac{A_{\mathrm{N1}}^{\mathrm{NL}}(2\omega)}{A_{\mathrm{M}}^{\mathrm{NL}}(2\omega)}$. The second part is related to the cumulative effect due to the MNP, in which $f(x)$ describes the attenuation of the cumulative Lamb wave components due to the wave divergence. Using *TNP*, the *SL* of the *TNP-x* curve can be expressed as

$$\begin{aligned} SL&=\frac{\dfrac{A_{\mathrm{N}}^{\mathrm{NL}}(2\omega)}{\left(A_{\mathrm{N}}^{\mathrm{L}}(\omega)\right)^{2}}-\dfrac{A_{\mathrm{M}}^{\mathrm{NL}}(2\omega)}{\left(A_{\mathrm{M}}^{\mathrm{L}}(\omega)\right)^{2}}}{\Delta x}=\frac{\dfrac{A_{\mathrm{N1}}^{\mathrm{NL}}(2\omega)+\left[\int_{\mathrm{M}}^{\mathrm{N}} k_{\mathrm{material}}\left(A^{\mathrm{L}}(\omega)\right)^{2}\mathrm{d}x\right]f(x)}{\left(A_{\mathrm{N}}^{\mathrm{L}}(\omega)\right)^{2}}-\dfrac{A_{\mathrm{M}}^{\mathrm{NL}}(2\omega)}{\left(A_{\mathrm{M}}^{\mathrm{L}}(\omega)\right)^{2}}}{\Delta x} \\ &=\frac{A_{\mathrm{M}}^{\mathrm{NL}}(2\omega)}{A_{\mathrm{M}}^{\mathrm{L}}(\omega)}\frac{\dfrac{1}{A_{\mathrm{N}}^{\mathrm{L}}(\omega)}-\dfrac{1}{A_{\mathrm{M}}^{\mathrm{L}}(\omega)}}{\Delta x}+\frac{\left[\int_{\mathrm{M}}^{\mathrm{N}} k_{\mathrm{material}}\left(A^{\mathrm{L}}(\omega)\right)^{2}\mathrm{d}x\right]f(x)}{\left(A_{\mathrm{N}}^{\mathrm{L}}(\omega)\right)^{2}\Delta x} \end{aligned} \tag{7}$$

The above expression shows that the *SL* slope is no longer a constant. Instead, it is affected by both the attenuation of the Lamb waves due to the wave divergence effect (the first term and the second term) and the material status (the second term). Particularly, the slope tends to be larger when the attenuation of Lamb waves becomes severer.

The above analyses surmise that the commonly-used *TNP* may lead to an imprecise prediction of the *SL* for the distributed nonlinearity on one hand and a false characterization of the localized nonlinearity on the other hand, due to the wave divergence in 2D cases. All in all, this may jeopardize the damage diagnosis in the cumulative effect-based SHM methods. Numerical

evidences will be given in later sections to ascertain the above theoretically predicted *SL* variations.

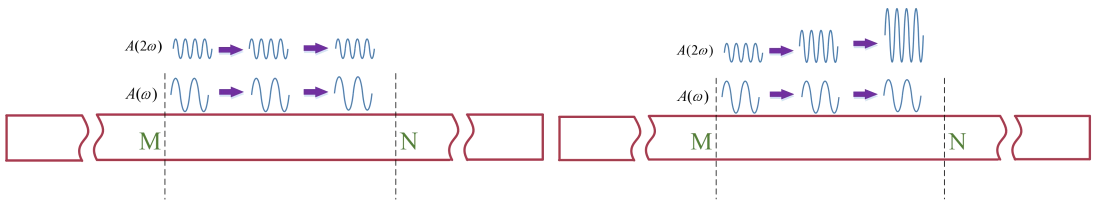

(a) (b)

Fig.1 Sketches of the propagating patterns of different wave components: (a) the AN (b) the MNP. (The amplitude of the second harmonic waves should be much smaller than that of the fundamental waves.)

2.3 A refined nonlinear parameter. To tackle the problem, a so-called "Refined Nonlinear Parameter (*RNP*)" is proposed based on the wave propagating characteristics as

$$RNP = \frac{A^{\mathrm{NL}}(2\omega)}{A^{\mathrm{L}}(2\omega)} \tag{8}$$

where $A^{\mathrm{NL}}(2\omega)$ is the amplitude of the second harmonic Lamb waves with the excitation at the fundamental frequency ω, $A^{\mathrm{L}}(2\omega)$ is the amplitude of the linear Lamb waves which are excited at the double frequency 2ω and propagate independently in the plate. Due to the wave divergence, the amplitude of the propagating second harmonic waves follows the same variation pattern as their linear counterparts at the double frequency so that the proposed *RNP* allows the compensation for the wave attenuation in 2D cases. Therefore, the physical nature of the proposed *RNP* is a compensated second harmonic wave descriptor, to be used as an alternative to the conventional β', which hopefully is more conducive to SHM applications.

As the AN-induced second harmonic Lamb waves propagate independently in the plate, their attenuation pattern should be similar to that of the linear Lamb waves at the double frequency.

Therefore, to characterize the AN according to Eq. (8), the *RNP* should be independent on the propagating distance and the slope of the *RNP*-*x* curve ($SL_{refined}$) should theoretically be zero. Compared with the *SL* obtained using the *TNP*, the non-damage related nonlinear source characterized with the *RNP* will no longer induce the false-positive cumulative effect.

As to the MNP, the $SL_{refined}$ can be expressed as

$$SL_{\text{refined}} = \frac{\dfrac{A_{\text{N}}^{\text{NL}}(2\omega)}{A_{\text{N}}^{\text{L}}(2\omega)} - \dfrac{A_{\text{M}}^{\text{NL}}(2\omega)}{A_{\text{M}}^{\text{L}}(2\omega)}}{\Delta x} = \frac{\dfrac{A_{\text{N1}}^{\text{NL}}(2\omega) + \left[\int_{\text{M}}^{\text{N}} k_{\text{material}} \left(A^{\text{L}}(\omega)\right)^2 \mathrm{d}x\right] f(x)}{A_{\text{N}}^{\text{L}}(2\omega)} - \dfrac{A_{\text{M}}^{\text{NL}}(2\omega)}{A_{\text{M}}^{\text{L}}(2\omega)}}{\Delta x} = \frac{\left[\int_{\text{M}}^{\text{N}} k_{\text{material}} \left(A^{\text{L}}(\omega)\right)^2 \mathrm{d}x\right] f(x)}{A_{\text{N}}^{\text{L}}(2\omega)\Delta x} \tag{9}$$

Eq. (9) indicates a positive slope so that the cumulative effect can still be characterized with the *RNP*. Moreover, compared with Eq. (7), the term which is merely related to the wave attenuation is eliminated (the first term in Eq. (7)). In another word, a better compensation for the wave attenuation in 2D cases can be achieved with the proposed *RNP*.

To sum up, in practical 2D cases with the presence of both the AN and the MNP in an SHM system, the proposed *RNP* is expected to pinpoint the cumulative effect from the measurements, which can only be induced by MNP. Meanwhile, the cumulative MNP-induced second harmonic Lamb waves can also be better characterized with the *RNP* through the proper compensation for the Lamb wave attenuation. These advantages can offer great benefit for the further SHM applications. The above analyses will be ascertained and validated in the following sections through numerical and experimental analyses.

3 Finite element validations

In this section, FE validations are carried out. To start with, the non-cumulative feature associated with the AN and the cumulative effect corresponding to the MNP are validated with 2D FE models under the plane wave assumption, laying out the benchmark for further discussions. Then, three-dimensional (3D) FE models are established to simulate typical nonplanar 2D wave propagating cases, along with a dedicated peak tracking method to extract the amplitude of the responses. Through analyses, the deficiencies of the *TNP* are addressed while the effectiveness of the proposed *RNP* are demonstrated.

3.1 Mechanism validations. As the foundation of the subsequent analyses, the propagating features of the AN-induced and the MNP-induced second harmonic Lamb waves need to be validated within our analytical framework. A 2D FE model is established to investigate the 1D propagating Lamb waves using ABAQUS, as illustrated in Fig. 2. Two piezoelectric actuators (20mm wide and 0.5mm thick) are symmetrically bonded on a 2mm-thick aluminum plate to generate S_0 mode Lamb waves. As to the wave sensing, five piezoelectric sensors (8mm wide and 0.5mm thick) are bonded on the plate from 100mm to 300mm away from the actuators, with a separation distance of 50mm between each pair. The thicknesses of the adhesive layers are all set to 0.03 mm. The nonlinear material properties of both the adhesive layer and the plate can be included or excluded as needed. The nonlinear material behaviors are programmed in the UMAT module. Relevant parameters of the piezoelectric transducers, adhesive layers and plate used in the FE models are tabulated in Table 1. The excitation is a 70kHz 5-cycle tone burst signal. The nonlinear responses are extracted in the time domain with the superposition method in which two signals with inverse phases are separately used as the excitations and their corresponding

responses are superposed [18]. The use of 5-cycle tone burst signal is to ensure a good temporal resolution, necessary for analyses. Since we use the S_0 Lamb waves in the low-frequency range, wave dispersion should be rather weak. Meanwhile, as the second harmonic Lamb waves are extracted using the superposition method in the time domain, only the wave amplitude matters instead of the cycles, which has more impact on the generation efficiency of the second harmonics.

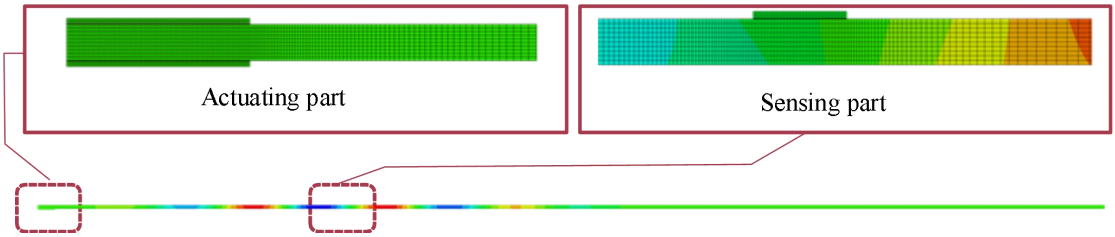

Fig. 2 The 2D FE model.

Table 1 Parameters used in the FE models.

PZT 5A					
Width	Thickness	E [1]*	v [1]*	d_{31}	e_{33}^{σ}
20mm/8mm	0.5mm	63.1 GPa	0.3839	-174 pm/V	1.51e-8 F/m
Bonding layer [2]*					
Thickness	E	v	A	B	C
0.03 mm	1.31 GPa	0.4	-20.9 GPa	-8.3Gpa	-6.1 GPa
Aluminum plate					

Thickness	*E*	*v*	*A*	*B*	*C*
2 mm	69.56 GPa	0.34	-702.4 GPa	-280.8 GPa	-205.6 GPa

Remarks: 1*. The elastic constants are equivalent parameters of piezoelectric material. 2*. The estimation of the nonlinear elastic constants of the bonding layer can be referred to [18].

First, only the AN is included in the model. As the amplitudes of the linear responses are much larger than their nonlinear counterparts, the overall responses of the sensors can be taken as the linear responses, as shown in Fig. 3(a). It can be seen that, apart from an offset in the time domain, the wave patterns as well as the amplitudes of the linear responses keep almost unchanged (the dotted line) during the wave propagation, as expected. Similar observation also applies to the nonlinear responses induced by the AN, as illustrated in Fig. 3(b). This shows the non-cumulative nature of the AN-induced nonlinear waves, as predicted in the theoretical analyses. Then, only the MNP is introduced to the system and the results are shown in Fig. 3(c). The amplitudes of the MNP-induced nonlinear Lamb waves increase gradually as indicated by the dotted line, demonstrating the typical cumulative effect within the chosen propagation region. Therefore, both the cumulative effect of the MNP and the non-cumulative effect of the AN are ascertained, which is consistent with the theoretical analyses.

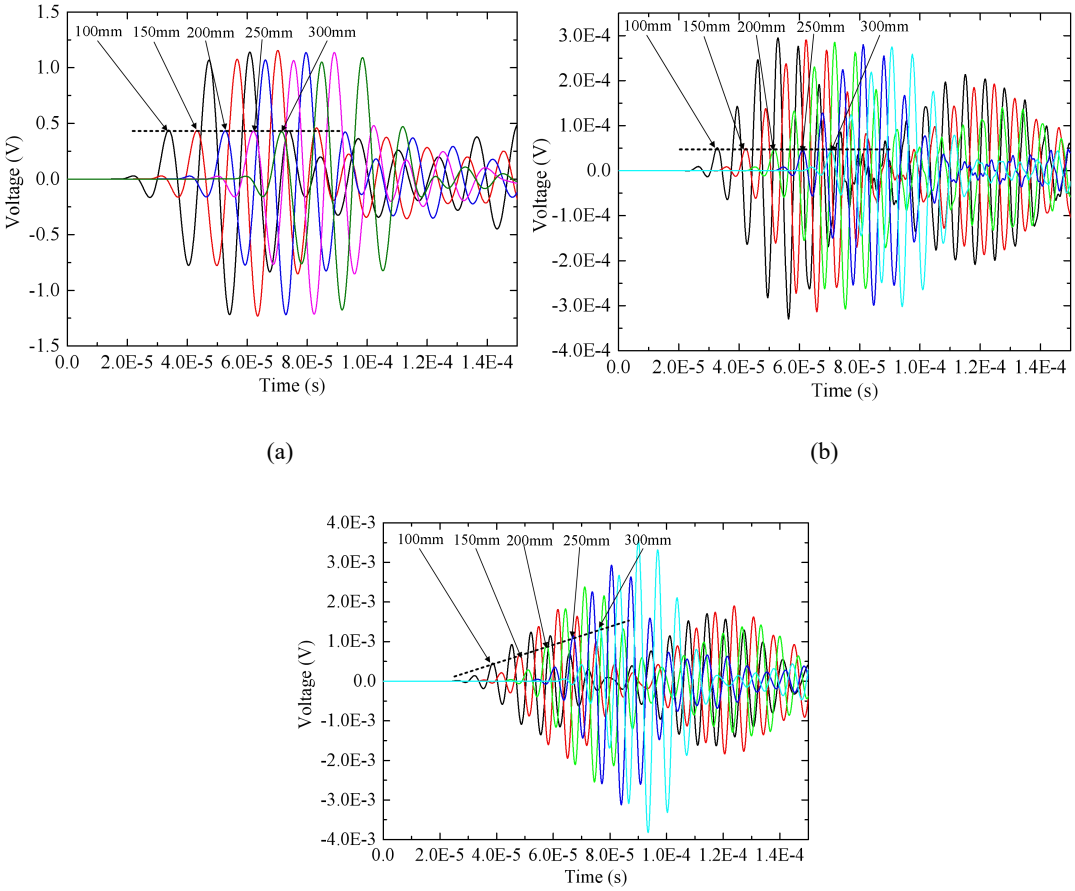

Fig. 3 Results of 1D cases: (a) overall (linear) responses; (b) nonlinear responses induced by the AN; (c) nonlinear responses induced by the MNP.

3.2 3D FE model and the peak-tracking method for amplitude extraction. To simulate the more practical 2D wave propagation cases, a 3D FE model is built with symmetric square piezoelectric actuators bonded on an aluminum plate as illustrated in Fig. 4. Only a quarter of the system is required with symmetric boundary conditions at the left and the bottom ends. Other details regarding the piezoelectric wafers (for both actuation and sensing) remain the same as those used in the above 1D case. In addition, the infinite elements are applied at the top edge of the plate to reduce the problem size and eliminate the edge reflections at the same time [27]. Again,

the AN and the MNP are separately introduced into the model as needed. Excitation frequencies at 70kHz or 140kHz with 5-cycle tone burst signals are used respectively.

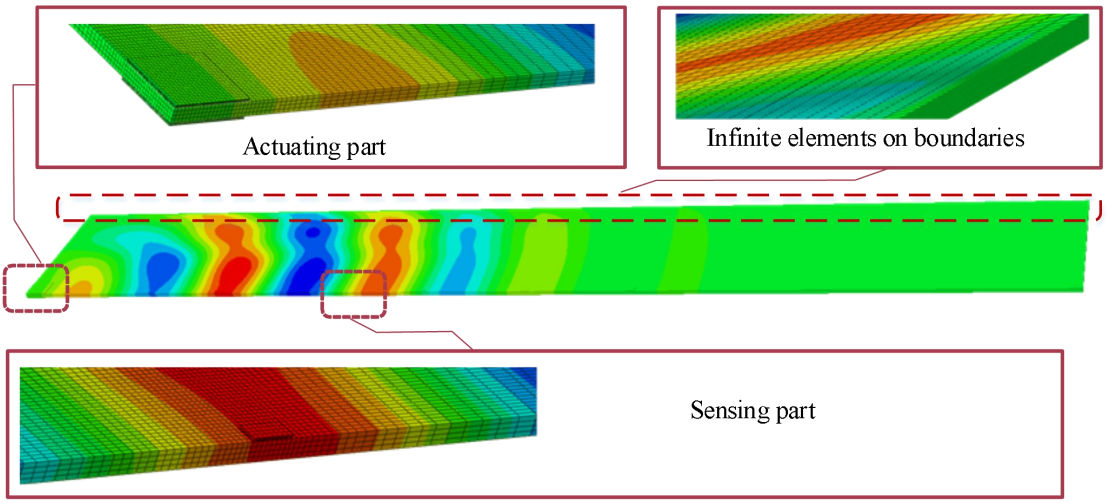

Fig. 4 The 3D FE model.

In the low-frequency range of our specific interest, reflections from the bonded sensors may be mixed with the incident Lamb waves since the wavelength and the distance between the sensors are comparable. In this case, traditional methods like the wavelet transform cannot precisely extract the amplitude of incident S_0 mode wave packages in the time-domain responses. Using the case of 140kHz excitation as an example, the voltage responses of five sensors are shown in Fig. 5(a). The complex Morlet wavelet transform would give the amplitudes of Lamb wave signals as shown in Fig. 5(b) [28]. It can be seen that the amplitude at 250mm is even larger than that at 200mm. This contradicts with the expected monotonically decreasing trend of the wave amplitudes associated with the divergence of Lamb waves. Nevertheless, as it takes some time for the reflections to be mixed with the incident waves, the very first parts of the S_0 mode Lamb wave signals in the time-domain tend to be less polluted. Based on this, a peak tracking method is

proposed to extract the amplitudes of Lamb wave responses by using the two amplitude quantities of the first obvious peak in the signal, marked by A and B in the example shown in Fig. 5(c). Through the normalization to the amplitude of the sensor output at 100mm away from the actuator, attenuation curves of Lamb waves at 140kHz are obtained and shown in Fig. 5(d). A relatively close agreement can be observed between the results obtained by peak tracking A and B. The average of the two is then used, showing a more physical and consistent decreasing trend of the wave amplitude as opposed to the one given by Morlet wavelet transform. It should be noted that the transient vibration and ringing effect may in principle exist [29]. In the present case, however, the captured signals show highly consistent and clear wave patterns and are well synchronized with the excitation frequency around the first two peaks. Therefore, the aforementioned phenomena, if any, should be negligible. In the following sections, this peak tracking method will be used to extract the wave amplitudes of various components as needed in the analyses.

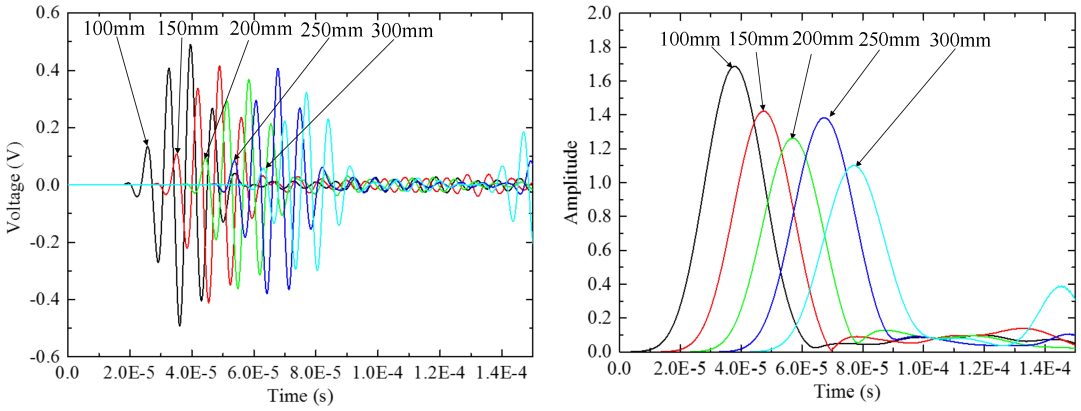

(a) (b)

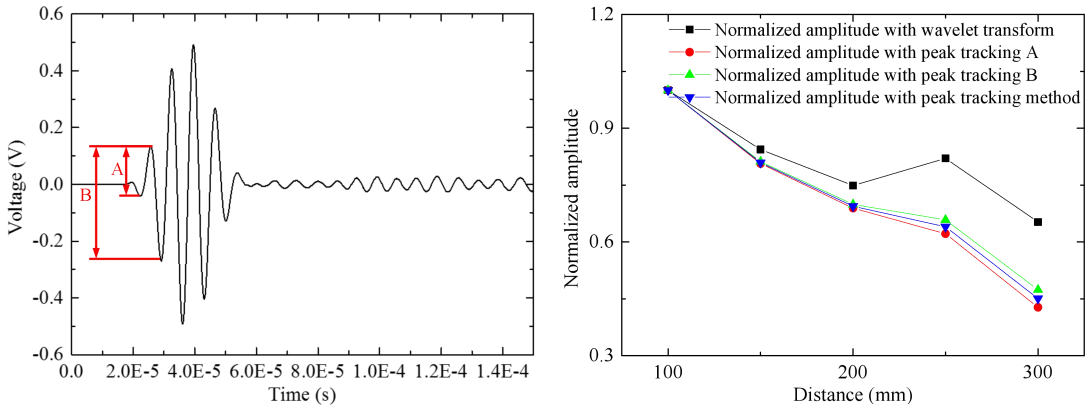

(c) (d)

Fig. 5 (a) The linear responses with 140kHz excitation; (b) the amplitudes of the Morlet wavelet coefficients of the linear responses; (c) strategy of the peak tracking method; (d) comparison of the amplitudes extracted with the wavelet transform and the peak tracking method.

3.3 Characterization of the second harmonic Lamb waves with *TNP* and *RNP* in 2D cases.

First, only the AN is introduced in the above 3D FE model. The excitation frequency is set to 70kHz and the linear voltage responses of the sensors at 100, 150, 200, 250 and 300mm are captured and shown in Fig. 6(a). The aforementioned peak tracking method is used, giving the comparisons shown in Fig. 6(b) between the wave attenuation at 70kHz and 140kHz. The similar decreasing trend for both cases agrees with the theoretical analyses in Section 2.1.

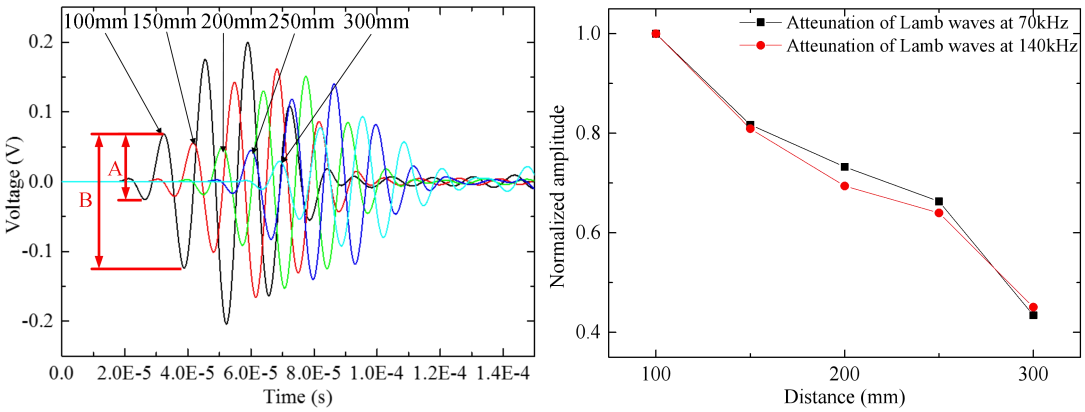

(a) (b)

Fig. 6 (a) Linear responses at 70kHz from the 3D FE model; (b) comparison of the wave attenuation between 70kHz and 140kHz cases.

The superposition method is then applied to extract the AN-induced second harmonic responses in the time domain. First, according the definition of the *TNP*, the AN-induced second harmonic voltage responses are compensated with the square of the linear wave amplitudes at 70kHz in Fig. 6 (b), resulting in the nonlinear responses of the sensors in the time domain as shown in Fig. 7(a). It is relevant to note that the values of the amplitudes have no physical meanings and only the trend of these nonlinear responses at different sensing positions is of interest. After further extracting the amplitudes of the responses and carrying out the normalization to the amplitude of the first sensor output, the normalized *TNP-x* figure is shown in Fig. 7(b). It can be seen that a false-positive cumulative effect indeed occurs as an artifact by the *TNP* in the present case where only the AN is considered. This is also consistent with the prediction of previous theoretical analyses.

To use the *RNP*, the Lamb waves are excited at 140kHz in a separate run. Then, the AN-induced second harmonic responses are compensated with the linear wave amplitudes at 140kHz, giving results shown in Fig. 7(c). Upon the further amplitude extraction and the normalization to the amplitude of the closest sensor signal, the normalized *RNP-x* figure is obtained and plotted in Fig. 7(d). The slope is very close to zero, truthfully indicating the non-cumulative nature of the AN.

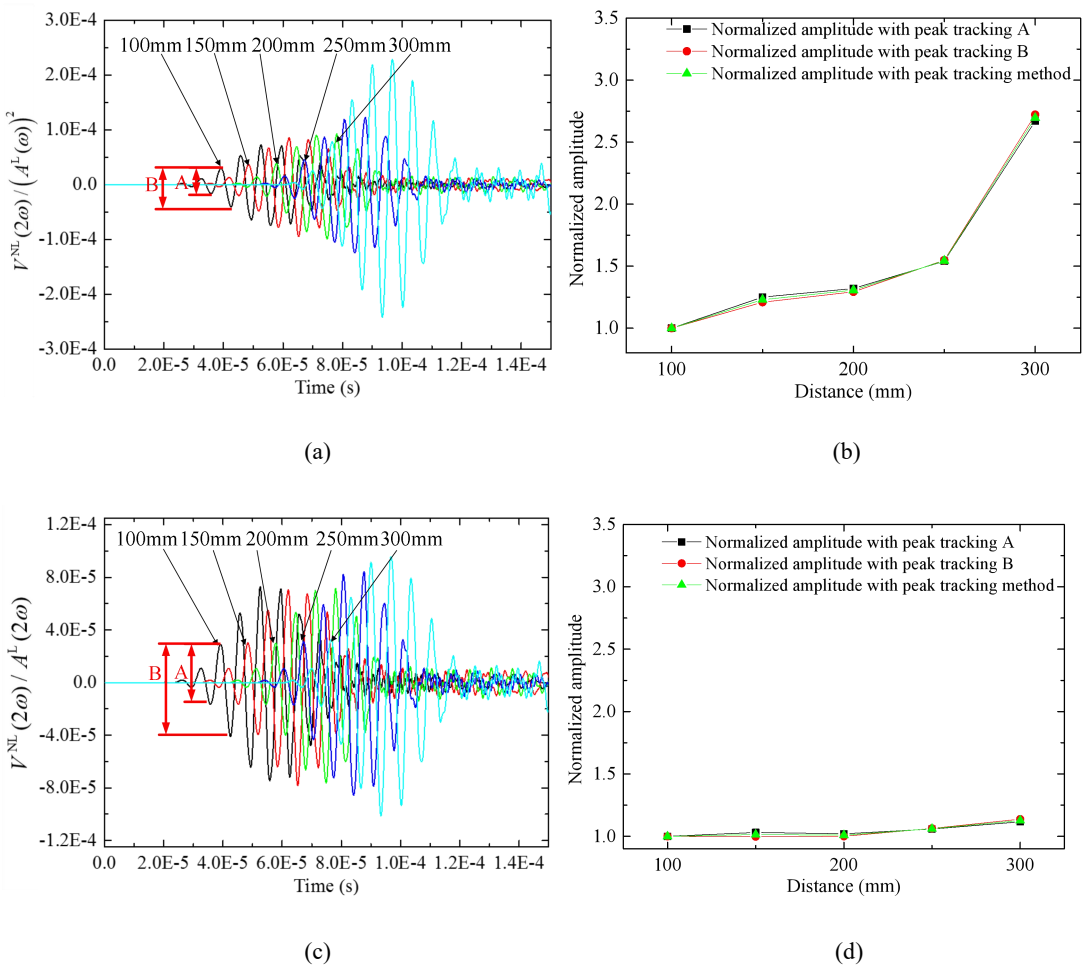

Fig. 7 (a) The AN-induced S_0 waves compensated with the square of the linear wave amplitudes at 70kHz according to the definition of the *TNP*; (b) the normalized *TNP-x* figure for the AN case; (c) The AN-induced S_0 waves compensated with the linear wave amplitudes at 140kHz according to the definition of the *RNP*; (d) the normalized *RNP-x* figure for the AN case.

Following the same process, only the MNP is introduced to the system. Both the *TNP* and the *RNP* are used to characterize the second harmonic responses, with the results shown in Fig. 8. The nonlinear responses after compensations are shown in Fig. 8(a) and (c), regarding to the *TNP* and *RNP*, respectively. By further extracting the wave amplitudes and carried out the normalization process, the normalized *TNP-x* figure and the normalized *RNP-x* figure are shown in Fig. 8(b) and

(d), respectively. Compared with the results using *TNP* (Fig. 8(b)), a better linear variation is obtained with the proposed *RNP* (Fig. 8(d)). This demonstrates that the wave attenuation is effectively compensated for when the *RNP* is used to characterize the MNP-induced second harmonic Lamb wave responses. This also agrees with the previous theoretical analyses.

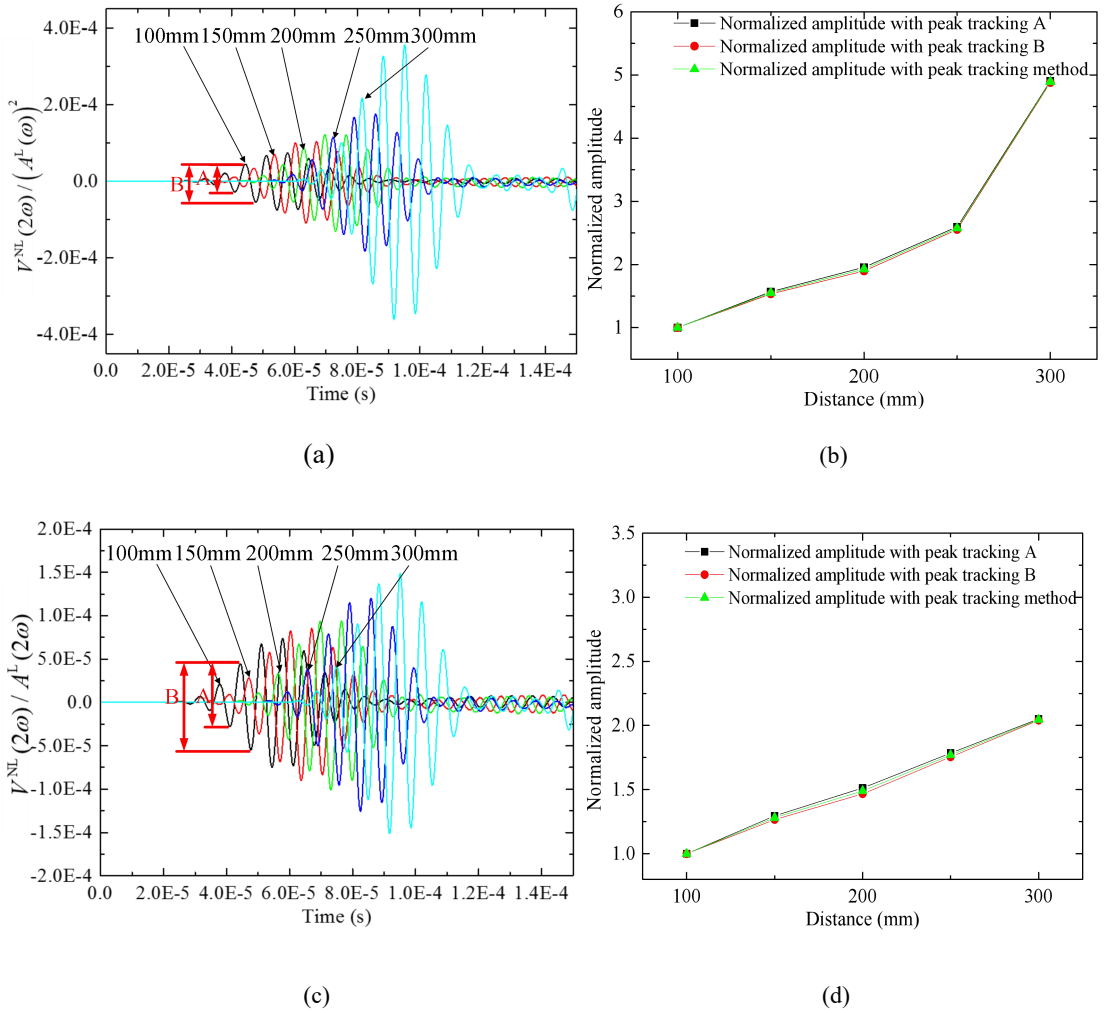

Fig. 8 (a) The MNP-induced S_0 waves compensated with the square of the linear wave amplitudes at 70kHz according to the definition of the *TNP*; (b) the normalized *TNP-x* figure for the MNP case; (c) The MNP-induced S_0 waves compensated with the linear wave amplitudes at 140kHz according to the definition of the *RNP*; (d) the normalized *RNP-x* figure for the MNP case.

To conclude, all the FE evidences support the previous theoretical analyses and demonstrate that the proposed *RNP* is more suitable for characterizing the nonlinear sources of different natures. First, the proposed *RNP* can effectively avoid the false-positive cumulative effect in the presence of the localized nonlinear sources such as the AN. Second, the cumulative effect due to the MNP can be better characterized with a fairly good linearity due to the appropriate compensation for the wave attenuation in 2D cases. Both outcomes should be beneficial to damage diagnosis in the cumulative effect-based SHM methods.

4 Experimental validations

The theoretically and numerically predicted advantages of the *RNP* are also experimentally validated. To this end, two typical system configurations are tactically conceived. Experiments are then carried out.

4.1 Design of the system configurations. In practical applications, both the AN and the MNP are inevitably present in a piezoelectric wafer-actuated SHM system. To experimentally validate the ability of the proposed *RNP* in characterizing and differentiating these two types of nonlinearities, two systems should be designed: the first one is referred to as the optimized system with dominant MNP and the other one the un-optimized system with more significant AN. The relative dominance level of the MNP can be achieved through manipulating the AN level in the system, which is materialized with the help of a previously developed model [18].

The level of the AN has been shown to be closely dependent on the size of the actuator as well as the excitation frequency due to the frequency tuning characteristics of the AN-induced S_0 mode Lamb waves [18]. The previously developed nonlinear shear-lag model allows accurate tuning and optimization of the actuator size for a given excitation frequency. In the present case, the optimized system corresponds to the valley of the frequency tuning curves, whilst the un-optimized one should be close to its peak. In the former, the AN is minimum, thus allowing the dominance of the MNP, whilst in the latter, the maximized AN exceeds and dominates the MNP. Without detailing the procedure, we design the configurations of the piezoelectric actuators for the fundamental frequency at 70kHz, giving the following two system configurations. The widths of the actuators are 32mm and 8mm for the optimized and un-optimized systems, respectively.

Before experiments, a 2D FE model is used again to ascertain the efficacy of the system design process. For this specific purpose, the piezoelectric actuators are only bonded on one side of the plate, to be in-line with the subsequent experiments. Configurations and material properties of the adhesive layers, the plates and piezoelectric sensors are identical to those used in the previous 2D FE model. The relative influences of the AN and the MNP are compared in terms of their corresponding nonlinear responses captured by the sensor located 200mm away from the actuator, as shown in Fig. 9. It can be seen that the AN is indeed dominant in the un-optimized system, as evidenced by its overwhelming amplitude as compared to that of the MNP (Fig.9(a)). In the optimized system, however, the level of the AN is significantly weakened, leading to a clear dominance of the MNP at the early part of the signals (S_0 mode Lamb wave responses).

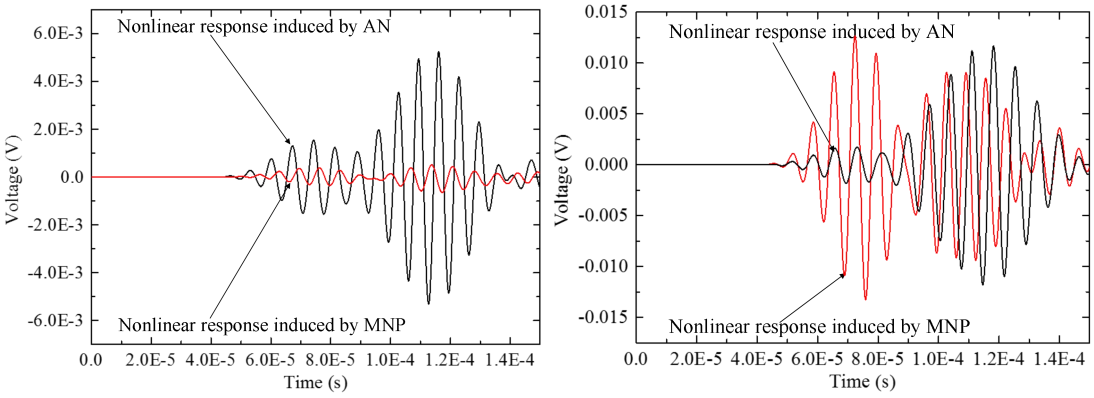

(a) (b)

Fig. 9 FE results: comparison between the influences of the AN and the MNP in the (a) un-optimized system; (b) optimized system.

4.2 Experimental set-up. In the experiments, six square piezoelectric wafers are bonded on a 2mm-thick aluminum plate, marked as A1, S1, S2, S3, S4 and A2, respectively, in Fig.10. The piezoelectric wafers are bonded by applying the same pressure to ensure the bonding conditions to be as consistent as possible. The marks and the geometric locations of the piezoelectric transducers are shown in Fig. 10(a). Actuator A1 has a width of 32mm and all the others are 8mm wide. The optimized system contains actuator A1 and sensors S1 to S4, in which the influence of the MNP should be dominant. The combination of actuator A2 and sensors S1 to S4 forms the un-optimized system in which the AN is expected to be more significant. The whole experimental set-up is shown in Fig. 10(b) with other details on the measuring system given in our previous work [18]. The excitation voltage is set to 200V. For each system configuration, the experiments are carried out following a two-step procedure:

1) Excite the system at 140kHz and capture the responses; use the peak track methods to extract the wave amplitudes;

2) Excite the system at 70kHz twice with inverse phases and capture the responses; extract the nonlinear responses with the superposition method and calculate the normalized *RNP-x* figure.

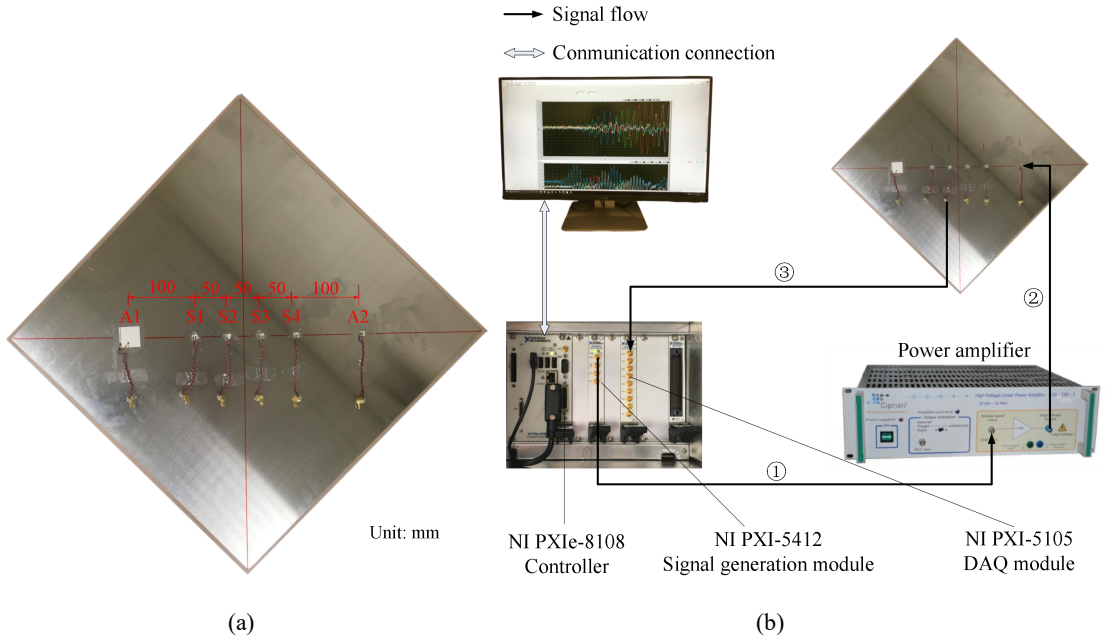

Fig. 10 (a) The test specimen with the actuators and sensors; (b) the sketch of the measurement system.

4.3 Results. The optimized system is first tested. Responses at 140kHz are first captured, as shown in Fig. 11(a). Using the peak tracking method, the corresponding attenuation curves are obtained and shown in Fig. 11(b). Then, the responses at 70kHz with the inverse excitations are superposed to obtain the nonlinear responses. 200 measurements are taken and averaged to minimize the influence of the background noise. Through the compensation with the linear wave amplitudes at 140kHz according to the definition of the *RNP*, the nonlinear responses of the sensors at different positions are shown in Fig. 11(c). After extracting the amplitudes with the peak tracking method and carrying out the normalization to the first amplitude, the normalized *RNP-x* figure is obtained and shown in Fig. 11(d). A clear cumulative effect can be observed from the results. This is consistent with our expectations that the influence of the MNP dominates in the

system.

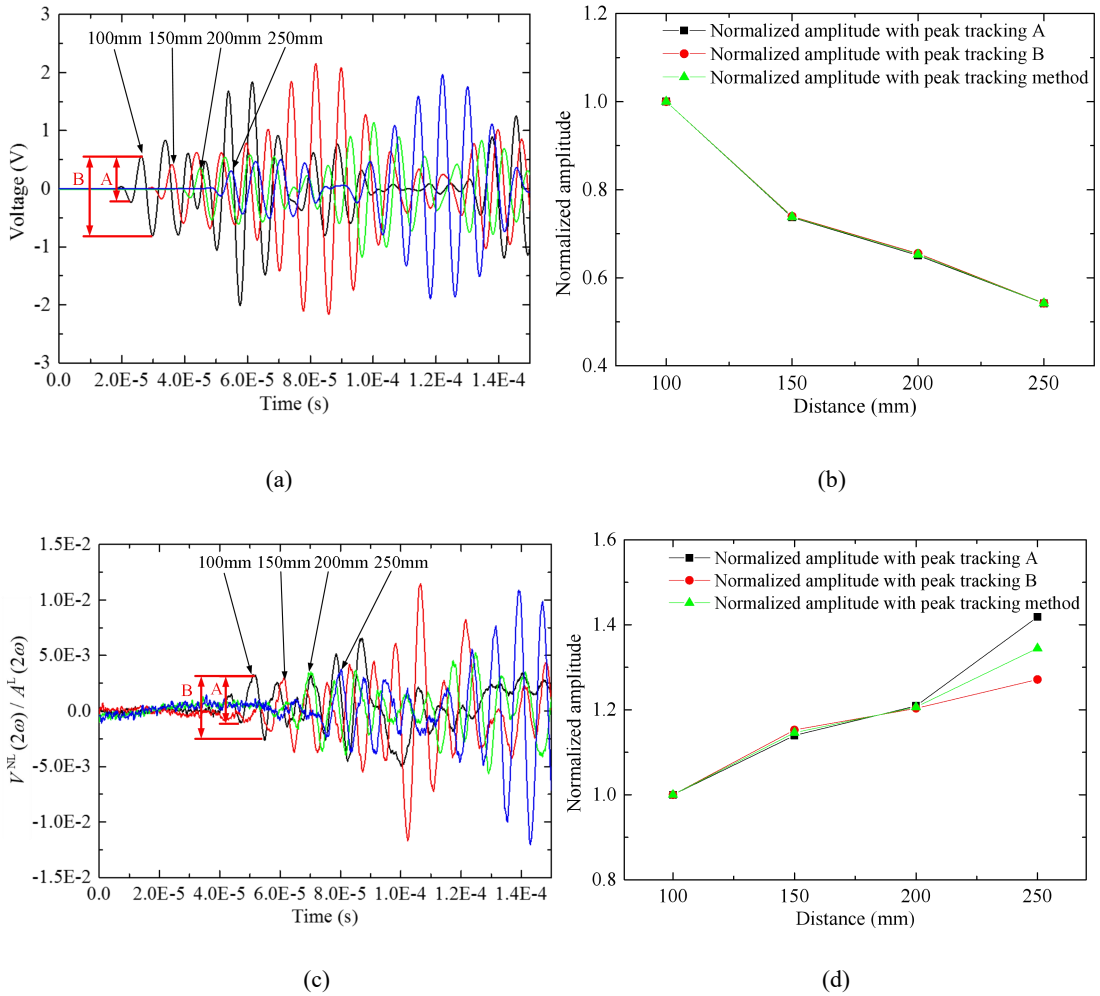

Fig. 11 Characteristics of the optimized system: (a) Linear responses of the sensor output at 140kHz; (b) attenuation of the linear Lamb waves at 140kHz; (c) the second harmonic Lamb responses compensated with the linear wave amplitudes at 140kHz according to the definition of the *RNP*; (d) the normalized *RNP-x* figure.

In the un-optimized system, following the same process, the linear responses and the attenuation curves of Lamb waves at 140kHz are shown in Fig. 12(a) and (b), respectively. Similarly, the nonlinear responses and the normalized *RNP-x* curve can be finally obtained, as

illustrated in Fig. 12(c) and (d). In this case, as the AN is dominant in the system, Fig. 12(d) shows no cumulative effect, which is also in agreement with our expectations.

To sum up, experimental evidences demonstrate that the proposed *RNP* can effectively characterize both AN-induced and MNP-induced second harmonic responses in terms of their cumulative characteristics in 2D cases, which should offer great benefit for further SHM applications.

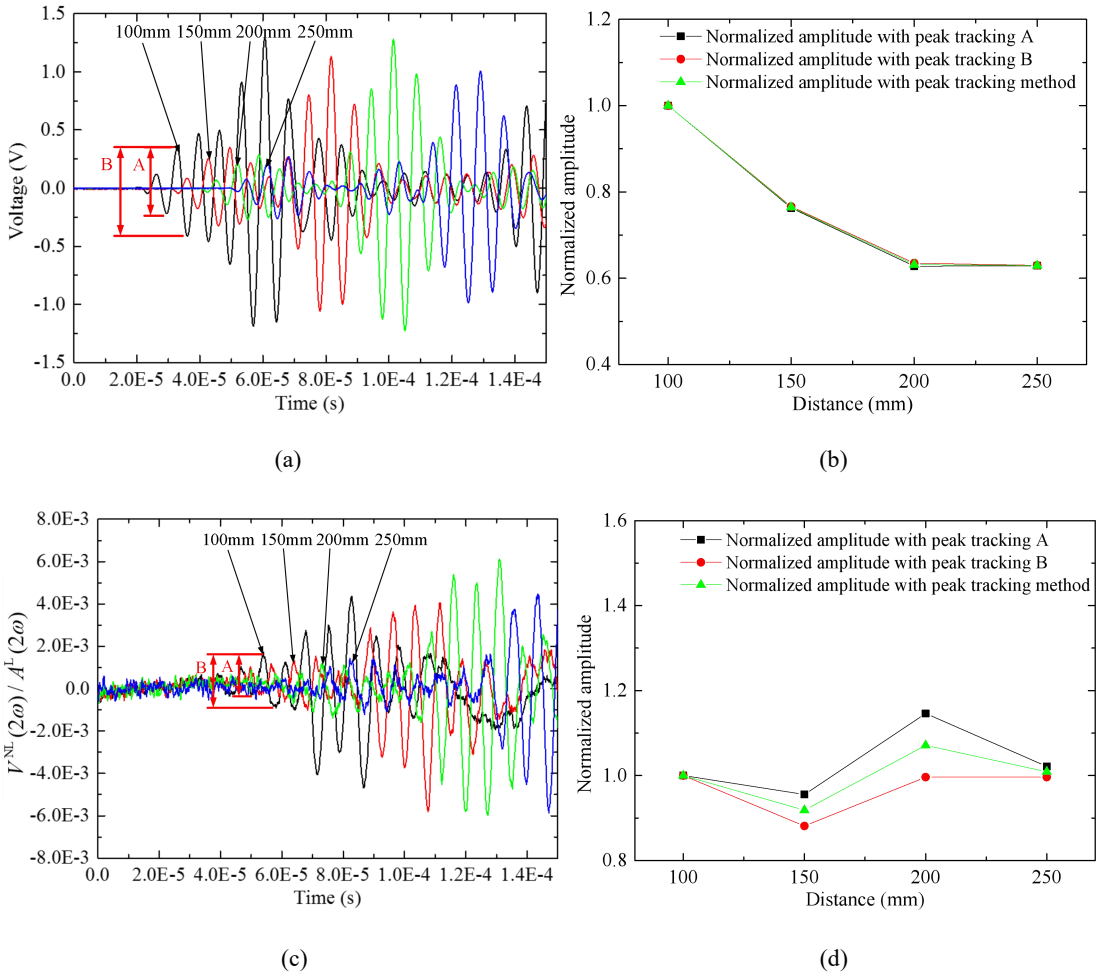

Fig. 12 Characteristics of the un-optimized system: (a) Linear responses of the sensor output at 140kHz; (b) attenuation of linear Lamb waves at 140kHz; (c) the second harmonic Lamb responses compensated with the linear wave amplitudes at 140kHz according to the definition of the *RNP*; (d) the normalized *RNP-x*

figure.

5 Conclusions

In this paper, the SHM-promising second harmonic Lamb waves in nonplanar 2D wave propagating cases are investigated in the perspective of their characterizations and quantifications. Under the assumption of the weak material damping in metallic plates, both the primary and the second harmonic undergo attenuations, dominated by the wave divergence. Theoretical analyses first show the deficiency of the widely-used traditional nonlinear parameter (*TNP*) to characterize the cumulative features of the second harmonic Lamb waves with changing measuring distances. As an alternative, a so-called refined nonlinear parameter (*RNP*) is proposed. The new parameter considers the wave propagating characteristics in a practical 2D configuration, aiming at a better characterization and differentiation of the localized and distributed nonlinear sources. A peak tracking method is used for wave amplitude extractions. The efficacy of the proposed *RNP* is then validated through the FE simulations in terms of characterizing both the cumulative effect associated with the MNP and the non-cumulative effect corresponding to the AN. Advantages of the proposed *RNP*, predicted by both theoretical and numerical analyses, are then experimentally validated using two tactically conceived systems with the help of a previously developed model. Through testing the two systems, the feasibility as well as the advantages of the proposed *RNP* are ascertained.

It is shown that the wave divergence of the Lamb waves in a nonplanar 2D configuration, along with the presence of the localized nonlinear sources, excites a vital influence on the

characterization of the cumulative effect of the second harmonic Lamb waves for SHM. This challenges the legitimacy and the accuracy of the *TNP* for the nonlinear wave characterizations and further for the cumulative effect-based SHM methods. By contrast, the proposed *RNP* is shown to entail a better characterization of the nonlinear sources of different natures in the system, as evidenced by both FE and experimental results. The advantages of the proposed *RNP* mainly lie in two aspects. First, using the *RNP*, the false-positive cumulative effect due to AN can be avoided, which is particularly appealing for further SHM applications; Second, the cumulative effect induced by the MNP can be better characterized with a fairly good linearity due to the proper compensation for the attenuation of the propagating Lamb waves.

The slope of the normalized *RNP*-*x* curve, derived from the proposed *RNP*, can be further extracted as an indicator for the detection of the microstructural changes in structures, since any changes in the slope can only be attributed to the material degradation of the plate other than other localized nonlinear sources such as the adhesive nonlinearity. Further investigations on the relevant SHM methods based on the newly proposed nonlinear parameter should be explored in our future work.

Acknowledgements

The authors wish to acknowledge a grant from Research Grants Council of Hong Kong Special Administrative Region (PolyU 152070/16E)

References

[1] Raghavan, A., and Cesnik, C. E., 2007, "Review of guided-wave structural health monitoring," Shock Vib. Dig., **39**(2), pp. 91–116.

[2] Su, Z., Ye, L., and Lu, Y., 2006, "Guided Lamb waves for identification of damage in composite structures: A review," J. Sound Vib., **295**(3), pp. 753-780.

[3] Yadav, S. K., Banerjee, S., and Kundu, T., 2013, "On sequencing the feature extraction techniques for online damage characterization," J. Int. Mater. Syst. Struct., **24**(4), pp. 473-483.

[4] Chillara, V. K., and Lissenden, C. J., 2016, "Review of nonlinear ultrasonic guided wave nondestructive evaluation: theory, numerics, and experiments," Opt. Eng., **55**(1), pp. 011002-011002.

[5] Matlack, K. H., Kim, J. Y., Jacobs, L. J., and Qu, J., 2015, "Review of second harmonic generation measurement techniques for material state determination in metals," J. Nondestruct. Eval., **34**(1), pp. 1-23.

[6] Muller, M., Sutin, A., Guyer, R., Talmant, M., Laugier, P., and Johnson, P. A., 2005, "Nonlinear resonant ultrasound spectroscopy (NRUS) applied to damage assessment in bone," J. Acoust Soc. Am., **118**(6), pp. 3946-3952.

[7] Van Den Abeele, K. E., Sutin, A., Carmeliet, J., and Johnson, P. A., 2001, "Micro-damage diagnostics using nonlinear elastic wave spectroscopy (NEWS)," NDT & E. Int., **34**(4), pp. 239-248.

[8] Liu, P., Sohn, H., Kundu, T., and Yang, S., 2014, "Noncontact detection of fatigue cracks by laser nonlinear wave modulation spectroscopy (LNWMS)," NDT & E. Int., **66**, pp. 106-116.

[9] Cantrell, J.H., and Yost, W.T., 2001, "Nonlinear ultrasonic characterization of fatigue microstructures," Int. J. Fatigue, **23**, pp. 487-490.

[10] Chillara, K. V., and Lissenden, C. J., 2012, "Interaction of guided wave modes in isotropic weakly nonlinear elastic plates: higher harmonic generation," J. Appl. Phys., **111**(12), pp. 124909.

[11] Deng, M., 1999, "Cumulative second-harmonic generation of Lamb-mode propagation in a solid plate," J. Appl. Phys., **85**(6), pp. 3051-3058.

[12] Deng, M., 2003, "Analysis of second-harmonic generation of Lamb modes using a modal analysis approach," J. Appl. Phys., **94**(6), pp. 4152-4159.

[13] Srivastava, A., and di Scalea, F.L., 2009, "On the existence of antisymmetric or symmetric Lamb waves at nonlinear higher harmonics," J. Sound Vib., **323**(3), pp. 932-943.

[14] Matsuda, N., and Biwa, S., 2011, "Phase and group velocity matching for cumulative harmonic generation in Lamb waves," J. Appl. Phys., **109**(9), pp. 094903.

[15] Liu, Y., Chillara, V. K., and Lissenden, C. J., 2013, "On selection of primary modes for generation of strong internally resonant second harmonics in plate," J. Sound Vib., **332**(19), pp. 4517-4528.

[16] Wan, X., Tse, P. W., Xu, G. H., Tao, T. F., and Zhang, Q., 2016, "Analytical and numerical studies of approximate phase velocity matching based nonlinear S0 mode Lamb waves for the detection of evenly distributed microstructural changes," Smart Mater. Struct., **25**(4), pp. 045023.

[17] Zuo, P., Zhou, Y., and Fan, Z., 2016, "Numerical and experimental investigation of nonlinear ultrasonic Lamb waves at low frequency," Appl. Phys. Lett., **109**(2), pp. 021902.

[18] Shan, S., Cheng, L., and Li, P., 2016, "Adhesive nonlinearity in Lamb-wave-based structural health monitoring systems," Smart Mater. Struct., **26**(2), pp. 025019.

[19] Pruell, C., Kim, J. Y., Qu, J., and Jacobs, L. J., 2007, "Evaluation of plasticity driven material damage using Lamb waves," Appl. Phys. Lett., **91**(23): pp. 231911.

[20] Deng, M., Wang, P., and Lv, X., 2005, "Experimental observation of cumulative second-harmonic generation of Lamb-wave propagation in an elastic plate," J. Appl. Phys., **38**(2), pp. 344.

[21] Hong, M., Mao, Z., Todd, M. D., and Su, Z., 2017, "Uncertainty quantification for acoustic nonlinearity parameter in Lamb wave-based prediction of barely visible impact damage in composites," Mech. Syst. Signal Pr., **82**, pp. 448-460.

[22] Xiang, Y., Zhu, W., Deng, M., Xuan, F. Z., and Liu, C. J., 2016, "Generation of cumulative second-harmonic ultrasonic guided waves with group velocity mismatching: Numerical analysis and experimental validation," EPL (Europhysics Letters), **116**(3), pp. 34001.

[23] Xiang, Y., Deng, M., Liu, C. J., and Xuan, F. Z., 2015, "Contribution of mixed dislocations to the acoustic nonlinearity in plastically deformed materials," J. Appl. Phys., **117**(21), pp. 214903.

[24] Pruell, C., Kim, J. Y., Qu, J., and Jacobs, L. J., 2009, "Evaluation of fatigue damage using nonlinear guided waves," Smart Mater. Struct., **18**(3), pp. 035003.

[25] Kim, J., Song, D. G., and Jhang, K. Y., 2017 "A method to estimate the absolute ultrasonic nonlinearity parameter from relative measurement," Ultrasonics, **77**, pp. 197-202.

[26] Konstantinidis, G., Drinkwater, B. W., and Wilcox, P. D., 2006 "The temperature stability of guided wave structural health monitoring systems," Smart Mater. Struct., **15**(4), pp 967-976.

[27] Satyarnarayan, L., Chandrasekaran, J., Maxfield, B., & Balasubramaniam, K., 2008, "Circumferential higher order guided wave modes for the detection and sizing of cracks and pinholes in pipe support regions," NDT & E. Int., **41**(1), pp. 32-43.

[28] Shan, S., Qiu, J., Zhang, C., Ji, H., and Cheng, L., 2016, "Multi-damage localization on large complex structures through an extended delay-and-sum based method," Struct. Health Monit., **15**(1), pp. 50-64.

[29] Liu, M., Kim, J. Y., Jacobs, L., and Qu, J., 2011, "Experimental study of nonlinear Rayleigh wave propagation in shot-peened aluminum plates—feasibility of measuring residual stress, " NDT & E. Int., **44**(1), pp. 67-74.